Lignosulfonate binders for green next-generation battery electrodes

Project Report (Final)

Summary of Results

Sodium lignosulfonate (LgSA) was tested as a binder for hard carbon anodes in sodium-ion batteries. It was compared with lignin (Lg), carboxymethyl cellulose (CMC), and alginate (Alg) binders, all of which apart from lignin are water-soluble. Electrochemical data demonstrates that LgSA appears to perform better even than CMC in three-electrode half-cells for both tested electrolytes 1 M $NaPF_6$ in PC or EC/DEC. The performance tends to be more stable in EC/DEC based electrolytes particularly for full cells, where the sodium metal counter electrode was replaced with a Prussian White cathode. Initial XPS results indicate a complex multi-layered SEI structure, which is dynamic in nature during discharge-charge cycling. It was found that mixing the LgSA with SBR results in an even greater performance for both electrolytes with a reasonable Coulombic efficiency. It is planned for at least one scientific article to be published from this work.

1. Introduction

A total of 500 kSEK was granted by ÅForsk to Uppsala University to carry out a project investigating the use of lignosulfonate binders in the fabrication of electrodes for rechargeable batteries. Such binders are thought to offer excellent structural stability, high water solubility, high ionic conductivity, facile extraction from wood pulp and are environmentally-friendly.

Researchers are trying to replace the most widely used poly vinylidene fluoride (PVDF) a conventional binder material for electrodes in commercial LIBs, to non-fluorinated environmentally friendly binders. Not only the presence of F in PVDF has inspired the community to come up with an alternate but also other issues such dissolution of F from the polymer during cycling of batteries as well as the reaction between PVDF and Li is exothermal which can cause self-heating and thermal runaway.(1,2) In this regard lignin which a by-product from Kraft pulp mills has been reported as cost effective eco-friendly binder by several groups for lithium-ion batteries.(3,4) One disadvantage with lignin as a binder is the usage of NMP, a hazardous and teratogenic solvent required to cast the electrode formulation. Several naturally available green binders which are water soluble have been reported in the literature for sustainable electrochemical energy storage.(5,6)

Our approach is to study sulfonated lignin salt as a binder as due to sulfonation lignin can be dissolved in water and makes a better alternative (from lignin to lignin sulfonate) green binder for energy storage. For this sodium lignosulfonate (LgSA) as a binder was considered along with the other aqueous binders, sodium carboxymethyl cellulose (CMC) and sodium alginate (Alg) for electrode processing. The binders are tested in sodium-ion batteries, which in the future may offer cost-effective and sustainable energy storage, for example in stationery energy storage where mass and volume are not so important as in mobile devices or electric vehicles. The Galvanostatic charge-discharge performance of hard carbon anode was investigated with LgSA, lignin (Lg), sodium carboxymethyl cellulose (CMC) and sodium alginate (Alg) in 3-electrode half cell as well full cell configuration.

2. Experimental Methods

2.1. ***Electrode preparation.*** Electrodes were prepared by mixing commercial hard carbon powder (Kuranode Type 3 lot K170921) and binder in the weight ratio of 95:5. Binders, LgSA, Alg and CMC used were purchased from Sigma-Aldrich, while Lg was obtained from Research Institutes of Sweden (RISE) as softwood kraft lignin. Commercially available styrene butadiene rubber (SBR) purchased from Sigma-Aldrich (**need to check**) was also used added in an equal weight ratio with LgSA binder (Hard carbon:LgSA:SBR 95:2.5:2.5) to fabricate hard carbon electrodes. The mixture of hard carbon and individual binder were converted into slurry by adding an appropriate amount of deionized water (DI) except lignin (NMP was used) and mixing over vortex homogenizer (Vortex® Genie2 from Scientific Industries). Using doctor blade slurry was cast over carbon-coated Al foil which was allowed to dry at ambient conditions for overnight and punched into 13 mm electrode which was further dried at 120 ºC in vacuum for 12 h. For full cell Prussian white (PW) was used as cathode whose synthesis is reported elsewhere.[7] PW as positive electrode were fabricated in an aforementioned way where it was mixed with Super P (Alfa Aesar®) and CMC (Sigma-Aldrich) binder in the ratio of 85:10:5 by weight in the mixture of 9:1 (v/v) DI: ethanol as solvent. Punched electrodes were dried at 140 ºC in vacuum for 24 h.

2.2. ***Electron microscopy.*** The dried electrodes of hard carbon (with 5% of binder by weight) were directly placed over carbon tape mounted on Al stub. SEM/EDS-Zeiss 1550 instrument was used to capture images at an operating acceleration voltage of 5.0 kV using in-lens detector.

2.3. ***Raman spectroscopy.*** Commercial hard carbon powder was mounted over a glass slide and pressed using another glass slide. Using Renishaw inVia Raman spectrometer, Raman spectrum was recorded utilizing a laser excitation wavelength of 532 nm.

2.4. ***Galvanostatic measurements.*** To gauge the electrochemistry of hard carbon mixed with four different binders, pouch cells were assembled in Glovebox (GS® Glovebox Systemtechnik) maintained at 0.3 ppm of O_2 and 0.2 ppm of H_2O levels under Ar atmosphere. Half cells, as well as full cells in three electrode configurations, were made using this hard carbon as working electrode in half cell, Prussian white as the positive electrode in full cell and a sodium metal disk as a reference electrode for half-cells as well as full-cells. Glass fibre separators (Whatman®) of 240 µm in thickness was used which was dried under vacuum to remove moisture from the pore. For the assembly of half cells, 14 mm diameter of metallic sodium disk (Aldrich 99.9% trace-metal basis) was used. The electrolyte used in the present study consisted of 1.0 M $NaPF_6$ (Stella) in propylene carbonate (PC, 99% Sigma Aldrich) and ethylene carbonate (EC, 99%, Sigma Aldrich)/diethyl carbonate (DEC, 99%, Sigma Aldrich) (1:1 v/v). was used as the electrolyte. For electrolyte preparation $NaPF_6$ salt was dried for 24 h under vacuum at 120 °C which was dissolved in PC and EC:DEC (soaked with molecular sieves, Sigma). 400-600 µL of the electrolyte was added during the pouch cell preparation which was finally sealed and kept under the resting period for 24 h. For Galvanostatic cycling, Biologic MPG2 potentiostat was used where the half cells and full cells were tested between 0.005 to 2 V and 1 to 4 V respectively, at C/5 C-rate. The theoretical capacity of commercial hard carbon is 300 mA h g^{-1}. For ex-situ XPS spectra, full cells in three-electrode configuration cells were fabricated using Celgard 2400 separator. Cells were stopped at 1st and 2nd charge as well as discharge conditions (voltage points for hard carbon 0.01 and 0.005 V during 1st and 2nd discharge, 1.49 and 1.53 V during 1st and 2nd charge).

2.5. ***X-ray Photoelectron Spectroscopy.*** The XPS measurements were performed on commercial hard carbon powder, pristine electrodes of hard carbon based upon various binder and cycled hard carbon mixed with LgSA. Spectra was recorded using PHI® 5500 spectrometer equipped with a monochromatic Al Kα radiation (1487 eV). Hard carbon powder was placed on an Indium substrate mounted over copper tape, pressed and tapped to remove loose particles. Pristine electrodes of hard carbon prepared using LgSA binder was mounted over copper tape and spectra were recorded. Similarly, for ex-situ XPS analysis full cells in three electrode configuration of hard carbon (counter electrode, CE) vs Prussian white (working electrode, WE) with a piece of Na as reference electrode were made and kept for 24 h rest time to stabilize the open-circuit voltage (OCV) after assembling. Then, cells were cycled and cycled hard carbon electrodes were immediately washed with dimethyl carbonate (DMC) solvent after dismantling stopped pouch cells. The software package CasaXPS was used for XPS peak fitting where energy calibration was performed by setting the binding energy for the adventitious carbon (C–C) in C 1s spectra to 284.8 eV.

3. Results

A commercial hard carbon powder was selected as an anode to investigate LgSA as a binder for SIBs. Raman spectra of the hard carbon powder showed the presence of D and G bands at 1343 and 1593 cm^{-1} revealing a disordered carbon material (**Figure 1a**).[8] An XPS survey spectrum (**Figure 1b**) revealed the presence of only C (C 1s 284.7 eV) and O (O 1s 533.0 eV). The Figure 1b inset presents the C 1s spectrum, fitted with peaks for sp^2 C (C=C) and sp^3 C (C-C) at binding energies of 284.69 and 284.90 eV, respectively. Other species (C-O 285.65 eV and C=O 290.36 eV) are due to surface functionalisation of the hard carbon.

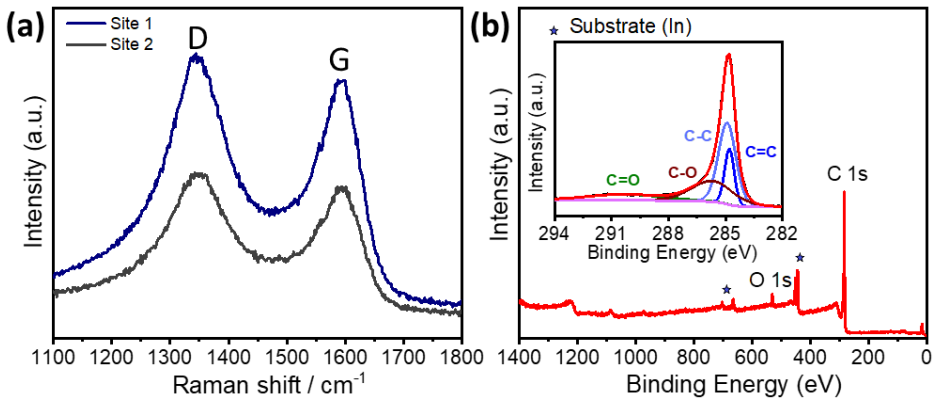

Figure 1. (a) Raman spectra of a commercial hard carbon powder using 532 nm excitation laser. (b) XPS survey spectrum of hard carbon confirming only C and O to be present; inset: peak-fitted C 1s spectrum.

SEM images of hard carbon electrodes fabricated with the different binders are shown in **Figure 2**. Despite the use of different solvents (water for LgSA, CMC and Alg; NMP for Lg), there appears to be insignificant difference in morphology for the different binders.

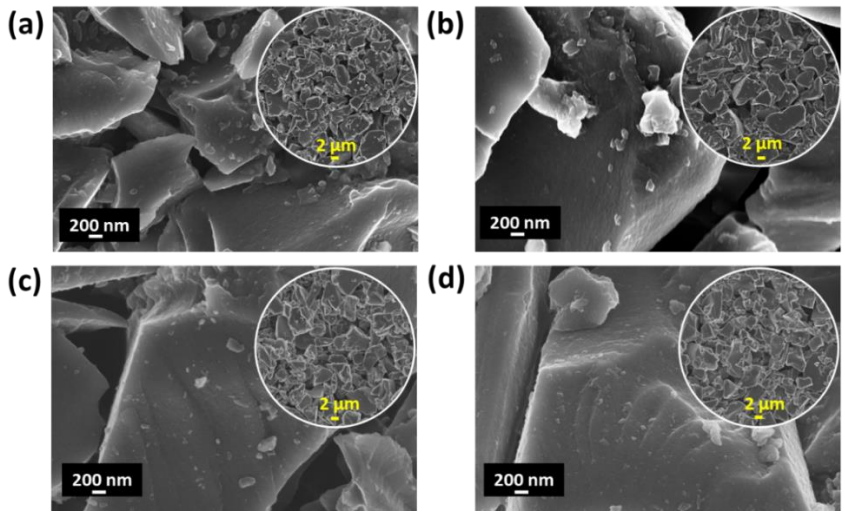

Figure 2. SEM image of pristine hard carbon electrodes using (a) LgSA, (b) Lg, (c) CMC and (d) Alg binders.

To investigate the influence of the different binders on sodium intercalation, electrochemical testing was performed using 3-electrode half-cells (with Na metal as counter and reference electrodes) and two different electrolyte systems. In **Figure 3**, the galvanostatic discharge and charge curves for the 1st and 10th cycles at C/5 C-rate are shown for $NaPF_6$ in PC and $NaPF_6$ in EC:DEC (1:1 wt. %) electrolytes. For the PC-based electrolyte, the 1st discharge (Na insertion) capacities of hard carbon using LgSA, Lg, CMC and Alg binders was found to be 244, 353, 266 and 320 mA h g^{-1}, respectively. The 1st charge (sodium removal) capacities for LgSA, Lg, CMC and Alg binders were found to be 222, 307, 237 and 295 mA h g^{-1}, respectively. The 10th discharge capacities for LgSA, Lg, CMC and Alg binders was found to be 299, 324, 277 and 280 mA h g^{-1}, respectively. The corresponding charge capacities for the 10th cycle for LgSA, Lg, CMC and Alg binders were 284, 322, 275 and 277 mA h g^{-1}, respectively. The capacity for the Lg electrode appears to be significantly higher than for the others.

For the EC:DEC-based electrolyte, the 1st discharge capacities using LgSA, Lg, CMC and Alg binders was found to be 282, 270, 286 and 306 mA h g^{-1}, respectively, while the corresponding charge capacities were 257, 238, 250 and 278 mA h g^{-1}, respectively. The 10th discharge capacities for LgSA, Lg, CMC and Alg binders were 253, 240, 206 and 280 mA h g^{-1}, respectively, while the corresponding charge capacities were 251, 239, 201 and 282 mA h g^{-1}, respectively. While the first cycle performance is very similar for each binder, the CMC electrode loses a significant amount of the initial capacity within 10 cycles. The capacities of hard carbon with LgSA binder in the EC:DEC electrolyte were found to be improved compared with the PC-based electrolyte. Also, there is no additional capacity can be observed in any binder when they cycled in $NaPF_6$/EC:DEC.

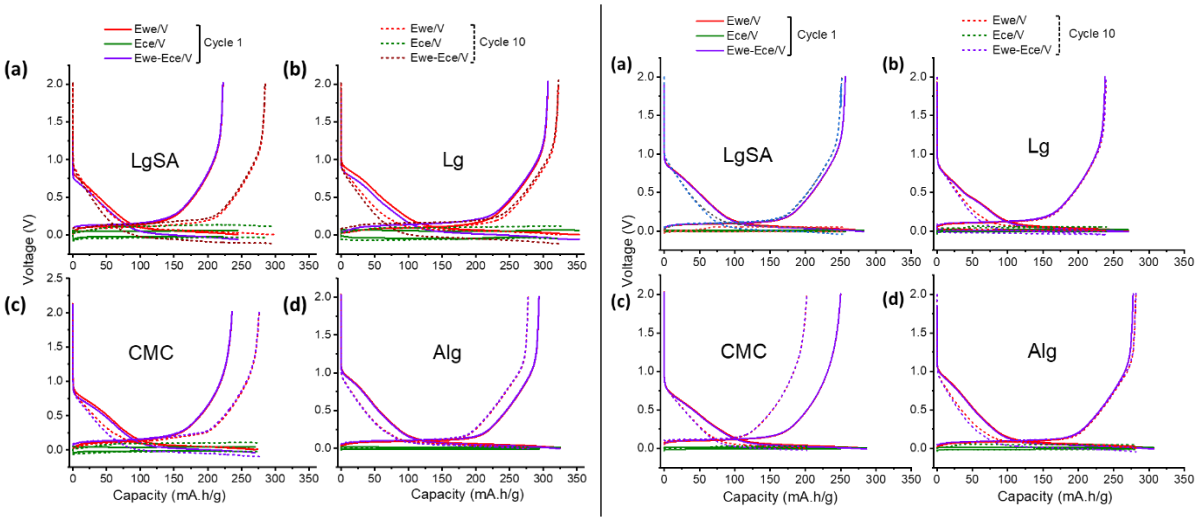

Figure 3. Voltage profiles for the 1st (solid line) and 10th (dashed line) galvanostatic cycles at C/5 rate of hard carbon in three-electrode half-cells binders (a) LgSA, (b) Lg, (c) CMC and (d) Alg using two electrolytes; *Left*: $NaPF_6$ in PC; *Right*: $NaPF_6$ in EC:DEC.

The galvanostatic cycling results for the different binders and electrolytes are summarised in **Figure 4**a and b with the Coulombic efficiencies (CE) presented in Figure 4c and d. For the PC-based electrolyte, the capacities drop in the initial cycles but then recover, especially so for LgSA and Lg, while for the EC:DEC electrolyte no such recovery is noticed. The LgSA and Lg binders show excellent stability over 10 cycles, while Alg exhibited higher capacities but also a degree of capacity fading. CEs for tests in PC electrolyte show close to 100 %, while there is a greater distribution of values for the EC:DEC electrolyte, with LgSA showing the poorest CE.

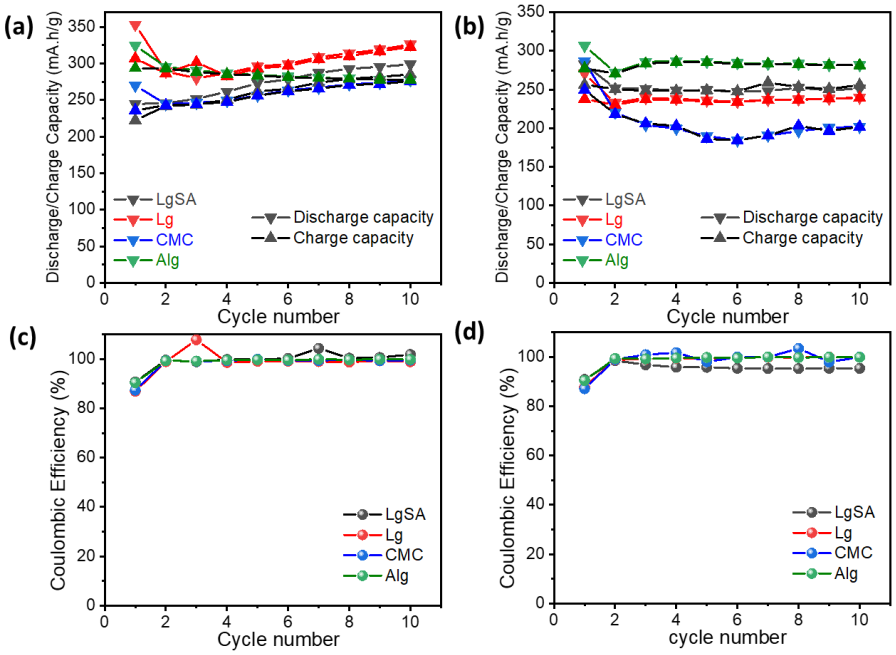

Figure 4. Cycling performance and Coulombic efficiency of hard carbon in three-electrode half-cells using different binders and electrolytes (a,c) $NaPF_6$ in PC and (b,d) $NaPF_6$ in EC:DEC electrolyte.

Figure 5 presents the voltage profiles of hard carbon anode (E_{ce}) using LgSA, Lg, CMC and Alg binders and the Prussian White cathode (E_{we}) individually versus the reference electrode in a 3-electrode full-cell configuration. The overall voltage of the full cell is shown in blue. First cycle discharge capacities for the hard carbon using LgSA, Lg, CMC and Alg binders using the PC-based electrolyte were 112, 129, 142 and 137 mA h g^{-1}, respectively, and 115, 126, 140 and 135 mA h g^{-1} for 10th cycle, respectively. For the EC:DEC-based electrolyte, first cycle discharge capacities were 129, 97, 121, and 136 mA h g^{-1}, respectively for LgSA, Lg, CMC and Alg binders for the first cycle and 125, 92, 125 and 131 mA h g^{-1}, respectively after 10 cycles.

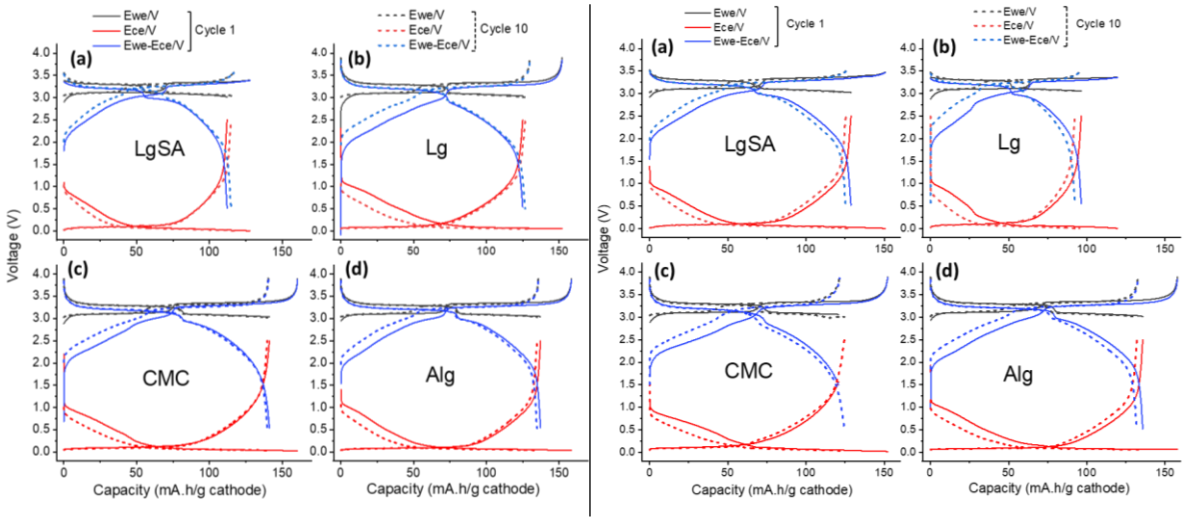

Figure 5. Voltage profiles for the 1st (solid line) and 10th (dashed line) galvanostatic cycles at C/5 rate of hard carbon in three-electrode full cell configuration (PW as cathode) using different binders (a) LgSA, (b) Lg, (c) CMC and (d) Alg using electrolytes; Left: $NaPF_6$/PC. Right: $NaPF_6$/EC:DEC.

The full-cell cycling is summarised in **Figure 6**a and b and the CE in Figure 6c and d, which was found to approach ~99% after the first cycle.

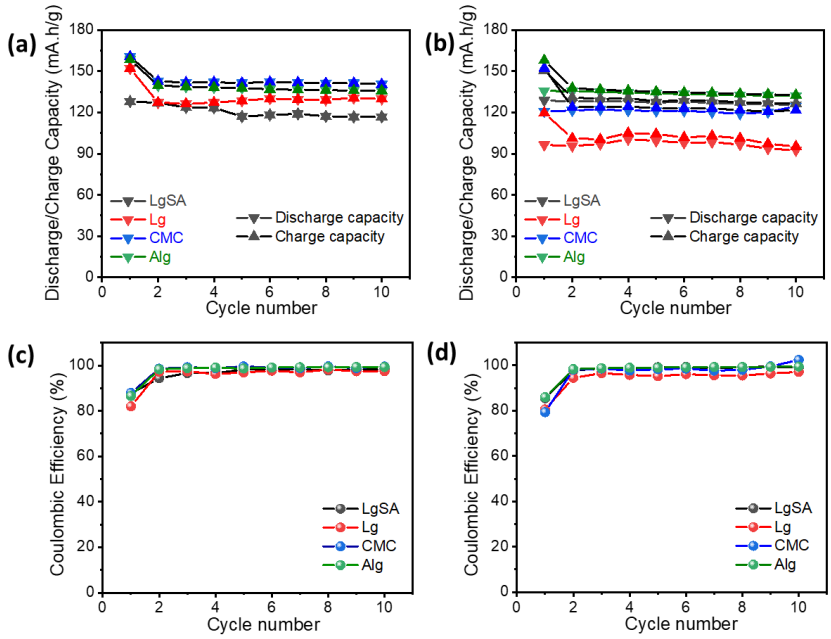

Figure 6. Cycling performance and the corresponding Coulombic efficiencies (CE) of hard carbon in three-electrode full-cell configuration using different binders with PW as positive electrode in (a) $NaPF_6$ in PC and (b) $NaPF_6$ in EC:DEC electrolytes.

Long-term cycling of the hard carbon with LgSA binder in a full cell with PW demonstrates good stability (**Figure 7**) in $NaPF_6$/PC and $NaPF_6$/EC:DEC electrolytes. However, the capacity fading was more noticable for the PC-based electrolyte. Red curves in Figure 7 (a,b) shows the hard carbon contribution in the full cell where the discharge capacity of the anode was fading from 128 to 95 mA h g^{-1} in $NaPF_6$/PC (Figure 7a) and from 151 to 122 mA h g^{-1} in $NaPF_6$/EC:DEC electrolyte (Figure 7b). Corresponding cycling of the full cell in $NaPF_6$/PC and $NaPF_6$/EC:DEC electrolytes is shown in Figure 7c and d, respectively, which suggest superior galvanostatic cycling of hard carbon anode with LgSA binder in EC:DEC solvent with minimal capacity fading for 45 cycles.

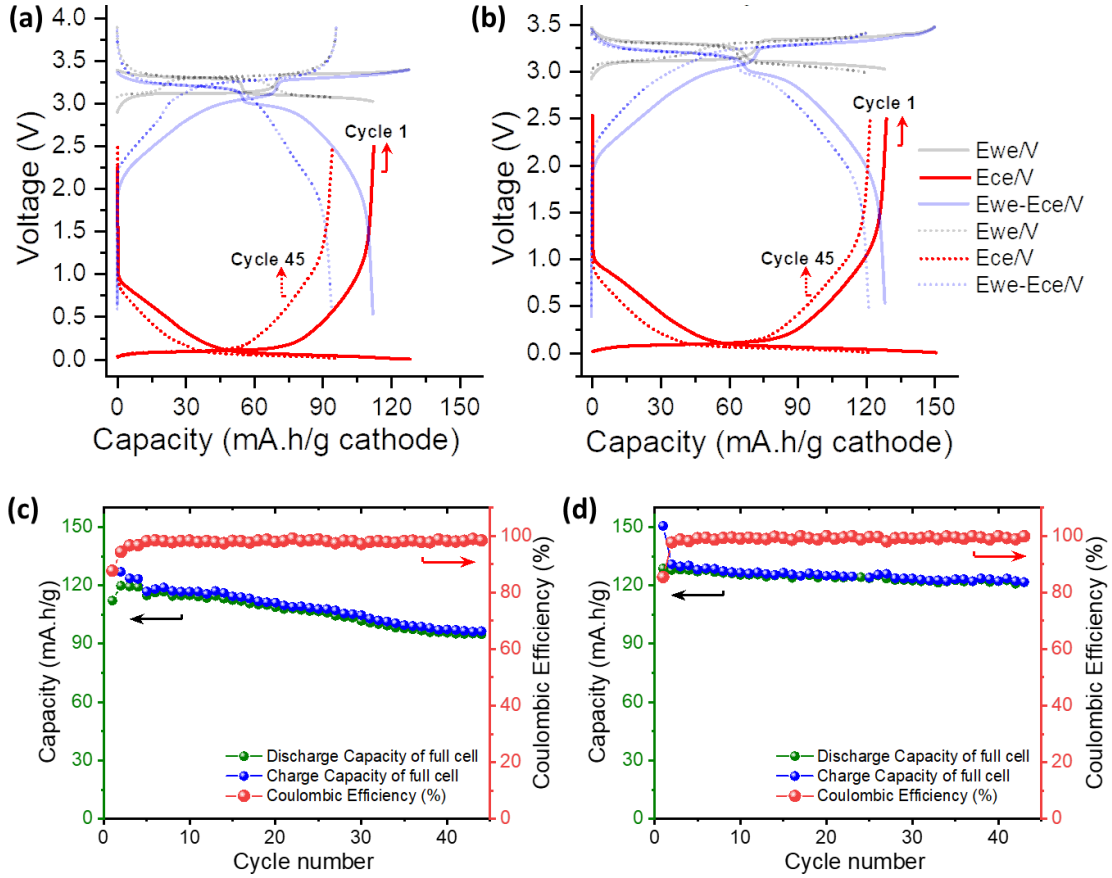

Figure 7. Voltage profile of hard carbon using LgSA binder in three electrodes full cell configuration with PW as cathode for the 1st (solid line) and 45th (dashed line) galvanostatic cycle in (a) $NaPF_6$/PC and (b) $NaPF_6$/EC:DEC electrolyte at C/5 rate. The corresponding cycling performance and Coulombic efficiency with LgSA binder is shown in (c) $NaPF_6$/PC and (d) $NaPF_6$/EC:DEC electrolytes.

Figures 8 and 9 present X-ray photoelectron spectroscopy data for electrodes in the pristine state as well as after "1st discharge" (sodiation of the hard carbon), "1st charge" (desodiation of hard carbon), "2nd discharge" and "2nd charge". The spectra for the pristine electrode show peaks mainly for hard carbon and the binder (C=C, C-C, C-O, C=O) in C 1s and O 1s as well as sodium in Na 1s and sulfur in S 2p spectra. On initial sodiation, mainly organic compounds in the C 1s and O 1s spectra are detected, while the C=C peak for hard carbon has disappeared. This can be attributed to the hard carbon being buried under a thick (> 10 nm) SEI surface layer. On desodiation, a strong peak for fluorine (F 1s) is visible and sulfur signals also are present again. This may indicate a multi-layered SEI, in which the organic surface components are oxidised during 'charge', revealing the fluorine-rich inorganic layer beneath, closest to the hard carbon surface. This is corroborated by the re-appearance of the hard carbon peak in C 1s. Similar observations are made on 2nd discharge and 2nd charge, indicating the dynamic nature of the SEI during charge-discharge cycling. Further work is required here to fully understand the structure of the SEI and it's stability over long-term cycling.

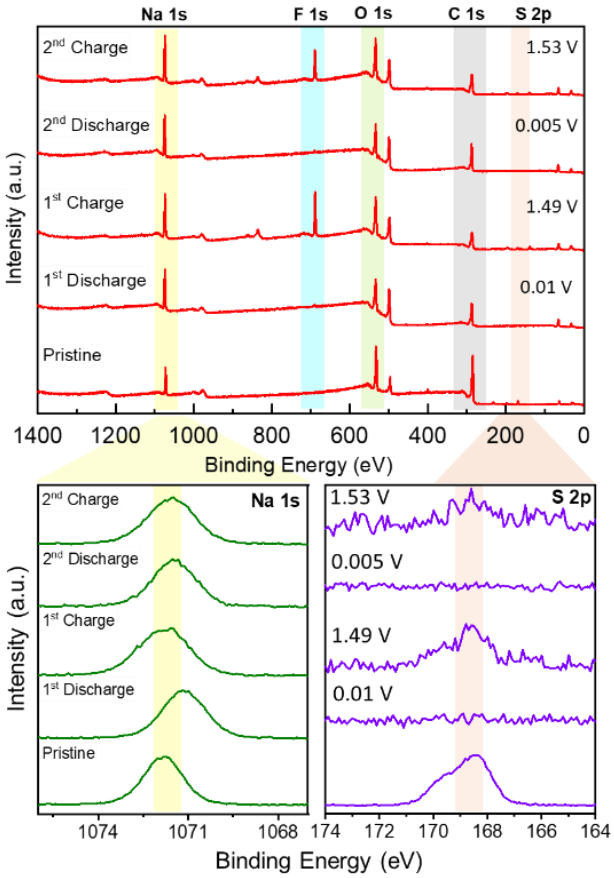

Figure 8. XPS survey spectra (top), Na 1s (bottom left) and S 2p (bottom right) peaks for pristine LgSA and cycled electrodes of LgSA binder in $NaPF_6$/EC:DEC electrolyte.

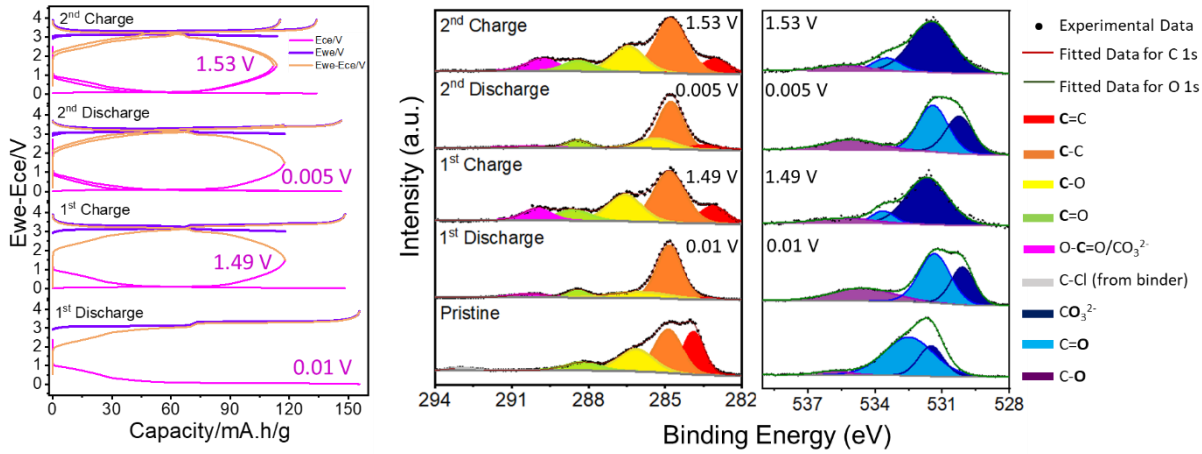

Figure 9. LgSA electrodes cycled to different potentials with their corresponding ex situ XPS plot for C 1s and O 1s in $NaPF_6$/EC:DEC.

In a further study, LgSA binder was mixed with SBR in equal weight ratio and the electrochemistry of hard carbon anode using LgSA + SBR binder investigated. In **Figure 10**a and b, the voltage curves for hard carbon using LgSA + SBR in a 3-electrode half-cell

configuration and $NaPF_6$/PC and $NaPF_6$/EC:DEC electrolytes are shown. In $NaPF_6$/PC, (Figure 10a) a discharge capacity of 242 mA h g^{-1} for the 1st cycle fades to 222 mA h g^{-1} for 10th galvanostatic cycle. Similar results were observed for the $NaPF_6$/EC:DEC electrolyte (Figure 10b) where the 1st and 10th discharge capacities are 239 and 223 mA h g^{-1}, respectively. The most promising results were obtained for full cell in 3 electrode configuration delivering a full cell discharge capacity of 132 and 128 mA h g^{-1} for 1st and 45th cycle at C/5 rate in $NaPF_6$/PC, as shown in Figure 10c. For $NaPF_6$/EC:DEC electrolyte, a promising capacity retention was observed in full cell where a discharge capacity fades from 140 to 135 mA h g^{-1} from 1st to 45th cycle at C/5 rate.

The corresponding cycling performance as well as Coulombic efficiency of hard carbon electrodes using LgSA + SBR binder in half cell as well full cell are shown in **Figure 11**. The Coulombic efficiency of hard carbon electrodes with LgSA + SBR binder in $NaPF_6$/PC and $NaPF_6$/EC:DEC electrolyte was found to be almost 99 % for half cell and full cell configurations. Figure 11c and d show excellent capacity retention without significant capacity fading for 45 cycle in full cell in both $NaPF_6$/PC and $NaPF_6$/EC:DEC electrolytes.

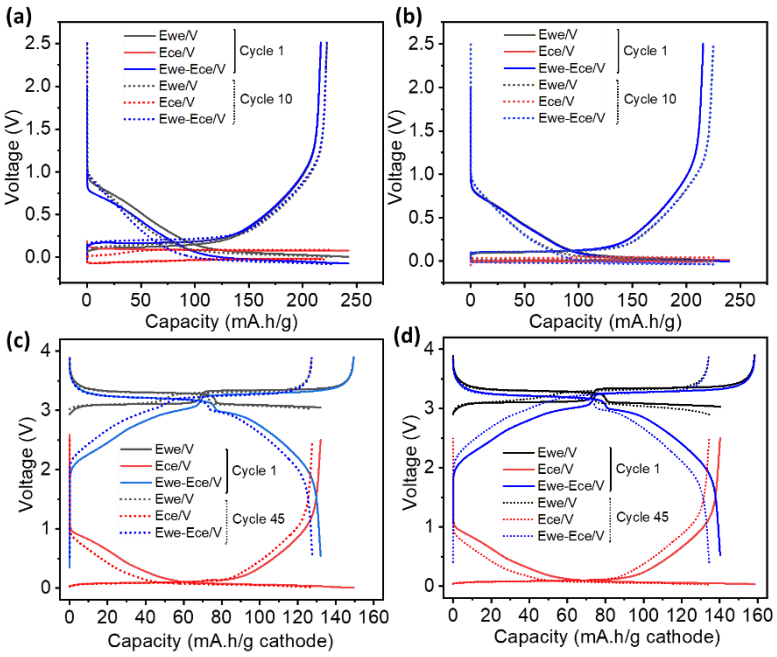

Figure 10. Voltage profile for the 1st (solid line) and 10th (dashed line) galvanostatic cycle of LgSA binder mixed with SBR in three electrode half-cell configuration cycled at C/5 rate in (a) $NaPF_6$/PC and (b) $NaPF_6$/EC:DEC electrolyte. Galvanostatic charge discharge curves for the 1st (solid line) and 45th (dashed line) cycle of LgSA binder mixed with SBR in three electrode full-cell configuration (PW as cathode) at C/5 rate in (c) $NaPF_6$/PC and (d) $NaPF_6$/EC:DEC electrolyte.

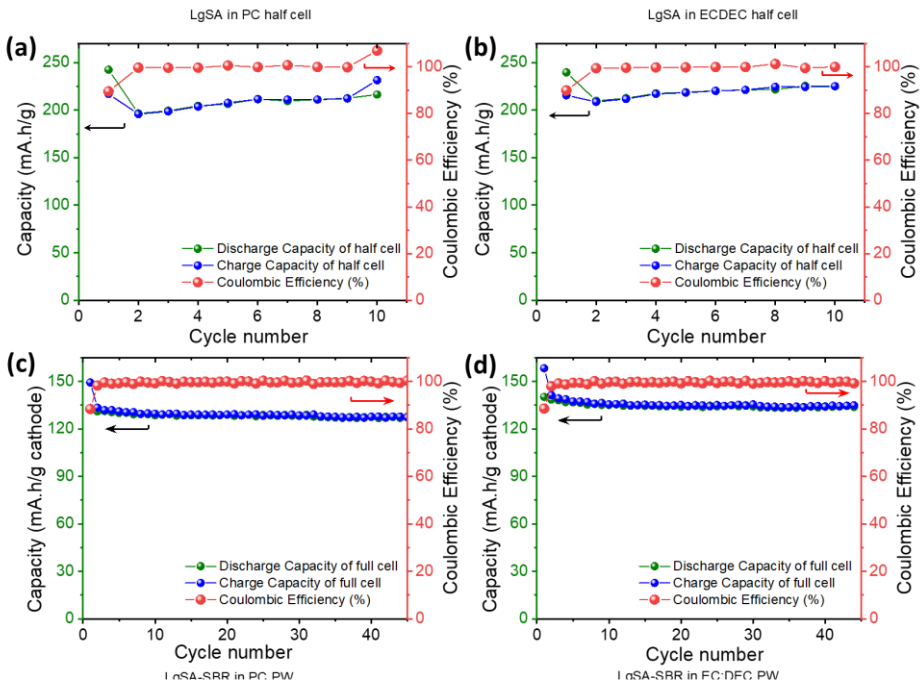

Figure 11. Cycling performance and Coulombic efficiency of hard carbon electrode (three electrode half cell) with LgSA + SBR binder in (a) $NaPF_6$/PC and (b) $NaPF_6$/EC:DEC electrolyte. Cycling performance and Coulombic efficiency of hard carbon electrode (three electrode full cell using PW as cathode) with LgSA + SBR binder to 45th cycle in (c) $NaPF_6$/PC and (d) $NaPF_6$/EC:DEC electrolyte.

Conclusions

Sodium lignosulfonate was tested as a binder for hard carbon anodes in sodium-ion batteries. It was compared with lignin, carboxymethyl cellulose (CMC), and alginate binders, all of which apart from lignin are water-soluble. Both LgSA and Lg exhibit different structures to the common polysaccharide-based structure of CMC and Alg. The LgSA appears to perform better even than CMC in three-electrode half-cells for both tested electrolytes 1 M $NaPF_6$ in PC or EC/DEC. The performance tends to be more stable in EC/DEC based electrolytes particularly for full cells, where the sodium metal counter electrode was replaced with a Prussian White cathode. Such a system and electrolyte was therefore selected to perform further XPS characterisation on. Initial XPS results indicate a complex multi-layered SEI structure, which is dynamic in nature during discharge-charge cycling. More work is required to establish firm conclusions on this. It was found that mixing the LgSA with SBR results in an even greater performance for both electrolytes with a reasonable Coulombic efficiency.

Project Outcomes

The successful use of lignosulfonate binder has been demonstrated for sodium-ion batteries, which, to the best of our knowledge, has not been reported before. This result will be published in a scientific article in the coming months. The comparison of the various different binders provides excellent knowledge to the group and wider scientific community. It is hoped that further work, particularly in the characterisation of the cycled electrodes, will be possible to gain a greater understanding of the SEI formation and evolution. It is also anticipated that the results of this project will be disseminated at conferences once travel to such events is possible again.

Acknowledgements

Naylor is grateful to ÅForsk for financially supporting this project and to Ritambhara Gond for performing the experiments and analysis of the results. Reza Younesi is also thanked for his assistance in the project and valuable discussions. StandUp for Energy is acknowledged for general financial support to the Ångström Advanced Battery Centre.

Financial Reporting

The following page gives an overview of the financial status of the project. Unfortunately, no trips could be made to perform experiments at synchrotrons or to conferences, due to the COVID-19 pandemic. Hence a larger proportion of the costs were made towards salary.

UPPSALA
UNIVERSITET

Institutionen för kemi, Ångström
Department of Chemistry,
Ångström Laboratory

Box 523
SE-751 20 Uppsala

Besöksadress/Visiting address:
Ångströmslaboratoriet
Lägerhyddsvägen 1

Datum **2020-10-01**

Ekonomisk redovisning

Projektnummer	139501924
Referensnr. ÅF	19-638
Projekttitel	Lignosulfonate binders for green next-generation battery electrodes

Ange total projektkostnad enligt kostnadsplanen i beslutet samt totalt upparbetade kostnader fr.o.m. projektets start:

	Upparbetade kostnader (kr)	
Lönekostnader	369 489	
Köpta tjänster		
Utrustning		
Material	1 624	
Laboratoriekostnad		
Resor		
Övriga kostnader		
Indirekta kostnader	128 887	
Summa	500 000	

T.o.m. vilket datum har kostnaderna upparbetats?	2020-09-30

Kommentarer

Skillnad mellan upparbetade kostnader och planerade kostnader (enligt beslut)

Indirekta kostnader avser lokalkostnader, overhead och IT-avgiften.

References

1. Pasquier A Du, Disma F, Bowmer T, Gozdz AS, Amatucci G, Pasquier A Du, et al. Differential Scanning Calorimetry Study of the Reactivity of Carbon Anodes in Plastic Li − Ion Batteries Differential Scanning Calorimetry Study of the Reactivity of Carbon Anodes in Plastic Li-Ion Batteries. 1998;145(2):472–7.

2. Maleki H, Deng G, Kerzhner-haller I, Anani A, Howard JN, Soc JE, et al. Thermal Stability Studies of Binder Materials in Anodes for Lithium − Ion Batteries Thermal Stability Studies of Binder Materials in Anodes for Lithium-Ion Batteries. 2000;147(12):4470–5.

3. Lu H, Cornell A, Alvarado F, Behm M, Leijonmarck S, Li J, et al. Lignin as a Binder Material for Eco-Friendly Li-Ion Batteries. Materials (Basel) [Internet]. 2016 Feb 25 [cited 2017 Sep 7];9(3):127. Available from: http://www.mdpi.com/1996-1944/9/3/127

4. Domínguez-Robles J, Sánchez R, Díaz-Carrasco P, Espinosa E, García-Domínguez MT, Rodríguez A. Isolation and characterization of lignins from wheat straw: Application as binder in lithium batteries. Int J Biol Macromol [Internet]. 2017 Nov 1 [cited 2019 Feb 25];104:909–18. Available from: https://www.sciencedirect.com/science/article/pii/S0141813017319153?via%3Dihub

5. Courtel FM, Niketic S, Duguay D, Abu-lebdeh Y, Davidson IJ. Water-soluble binders for MCMB carbon anodes for lithium-ion batteries. J Power Sources. 2011;196(4):2128–34.

6. Bresser D, Buchholz D, Moretti A, Varzi A, Passerini S. Alternative binders for sustainable electrochemical energy storage-the transition to aqueous electrode processing and bio-derived polymers. Energy Environ Sci. 2018;11(11):3096–127.